

Variable Radii Poisson-Disk Sampling

Scott A. Mitchell*

Alexander Rand†

Mohamed S. Ebeida‡

Chandrajit Bajaj§

Abstract

We introduce three natural and well-defined generalizations of maximal Poisson-disk sampling. The first is to decouple the disk-free (inhibition) radius from the maximality (coverage) radius. Selecting a smaller inhibition radius than the coverage radius yields samples which mix advantages of Poisson-disk and uniform-random samplings. The second generalization yields hierarchical samplings, by scaling inhibition and coverage radii by an abstract parameter, e.g. time. The third generalization is to allow the radii to vary spatially, according to a formally characterized sizing function. We state bounds on edge lengths and angles in a Delaunay triangulation of the points, dependent on the ratio of inhibition to coverage radii, or the sizing function’s Lipschitz constant. Hierarchical samplings have distributions similar to those created directly.

1 Maximal Poisson-disk Sampling

A *sampling* is a set of ordered points taken from a domain at random. Each point is the center of a disk that precludes additional points inside it, but points are otherwise chosen uniformly. The sampling is maximal if the entire domain is covered by disks. Together these define maximal Poisson-disk sampling (MPS).

More formally, a sampling $X = (\mathbf{x}_i)_{i=1}^n$, $\mathbf{x}_i \in \Omega$ satisfies the *inhibition* or *empty disk* property if

$$\forall i < j \leq n, |\mathbf{x}_i - \mathbf{x}_j| \geq r. \quad (1)$$

The set of *uncovered points* is defined to be

$$S(X) = \{\mathbf{y} \in \Omega : |\mathbf{y} - \mathbf{x}_i| \geq r, i = 1..n\}. \quad (2)$$

A sampling X is *maximal* if $S(X)$ is empty:

$$S(X) = \emptyset. \quad (3)$$

Given a non-maximal sampling, the next sample is *bias-free* if the probability of selecting it from any uncovered subregion is proportional to the subregion’s area, i.e.,

$$\forall A \subset S(X) : P(\mathbf{x}_{n+1} \in A | X) = \frac{|A|}{|S(X)|}. \quad (4)$$

*Sandia National Laboratories, samitch@sandia.gov

†Institute for Computational Engineering and Sciences, The University of Texas at Austin

‡Sandia National Laboratories

§Dept. of Computer Science and Institute for Computational Engineering and Sciences, The University of Texas at Austin

We generalize these equations: decoupling the radii in the empty disk and uncovered equations; scaling the radii for a hierarchy of denser samplings; and varying the radii spatially by a sizing function.

The purpose of this short paper is to introduce these generalizations in a mathematically consistent way. Examples illustrate the properties of the resulting output distributions. For simplicity our language is two-dimensional, e.g. “disks” instead of “spheres,” but the definitions are general dimensional. Also for simplicity, we consider only periodic (or free-boundary) domains. These domains are used in some applications: computer graphics texture synthesis and mesh generation of material grains.

2 Motivation and Previous Work

An MPS sampling is a separated-yet-dense point set: points are not too close together and lie throughout the entire domain. This is an efficient way to distribute a fixed budget of points.

In mesh generation, separated-yet-dense points yield Delaunay triangulations (DT) with provable quality bounds [4, 9, 19]. Delaunay Refinement (DR) [20] introduces points to improve DT triangle quality and a separated-yet-dense point set follows. Variations of DR provide adaptivity and sizing control [16]. DR is usually deterministic; although regions of acceptable points have been characterized [12, 13], and one may select from regions randomly to improve tetrahedron quality [5], randomized point positions are not a traditional *requirement*. However, random meshes are of independent interest for certain applications; e.g. in some fracture mechanics methods, cracks propagate only along mesh edges. Meshes from MPS produce more physically realistic cracks [1, 2, 8, 7]. Ensembles of MPS meshes can model natural material strength variations.

In a sphere packing no two disks overlap. If the disk radii satisfy a Lipschitz condition then a quality mesh results [19]. As in MPS and in reverse to DR, algorithms add disks until the packing is (nearly) maximal, and a good-quality DT follows. A fixed- r MPS sampling is a sphere packing; halve the disk radius r so no disks overlap. We define four new spatial variations for MPS, however none are equivalent to maximal sphere packings. Conflicts are defined by disks containing each other’s centers; for unequal radii this is not equivalent to non-overlapping $1/2$ -radii disks. Also, we achieve a

maximal distribution following a characterized statistical process.

MPS is popular for computer graphics [15] for texture synthesis because the distribution avoids repeating patterns of distances between points which produce visible artifacts. Fixed radius disks are traditional, but not suitable in all situations.

In real-time games and data exploration [17] with level-of-detail adaptivity, renderings use a finer sampling as the camera zooms in. Switching between discrete sets of samples is common, but has the potential to introduce visible artifacts or scene jumps [23]. Our definitions enable smoothly increasing density in time. Spatially varying samplings are useful for objects with varying curvature and lighting [3, 14]. Curvature and solution gradients motivate spatially-varying finite element meshes, and incremental adaptivity is preferred over mesh replacement.

Varying density sampling is popular in Graphics but often the algorithms are heuristic, and the requirements not well understood. This paper seeks to provide some formal guidance. For example, the spatially-varying sampling algorithm of Bowers et al. [3] uses a datastructure that holds all the nearby points whose Poisson-disks might conflict with a new point. This datastructure sometimes overflows in practice. We show that this is the fault of the input and not their algorithm: the **bigger-disks** criteria in Section 5 shows that a sizing function with Lipschitz constant $L < 1/2$ is necessary to bound the number of nearby points.

Classic dart throwing [6] generates samples and rejects those inside prior disks. The probability of generating an acceptable sample becomes vanishingly small, so maximality is not reached. After many rejected samples McCool and Flume [18] reduce the radii of disks, either locally or globally, to make room for more samples. An adaptive MPS variation [23] for deforming point clouds coarsens to remove points that are too close together, and refines to re-achieve maximality. For coarsening the disk-free and maximal criteria hold approximately, subject to a tolerance band. In Section 3 we effectively tune this tolerance band by the ratio of the two radii, and scale the radii continuously in Section 4.

3 Different inhibition and coverage radii

Here we relax the condition that the coverage and inhibition radii are equal. We focus on a particular relaxation that proves useful for generating hierarchical point sets, and flatter FFT radial power spectra.

Let $R_f \leq R_c$ denote the inhibition and coverage radii, respectively. The *empty disk* property is

$$\forall i < j \leq n, |\mathbf{x}_i - \mathbf{x}_j| \geq R_f. \quad (5)$$

The set of *free* points is defined to be

$$S(X) = \{\mathbf{y} \in \Omega : |\mathbf{y} - \mathbf{x}_i| \geq R_f, i = 1..n\}. \quad (6)$$

The set of *uncovered* points is defined to be

$$U(X) = \{\mathbf{y} \in \Omega : |\mathbf{y} - \mathbf{x}_i| \geq R_c, i = 1..n\}. \quad (7)$$

The sampling is *maximal* if $U(X)$ is empty,

$$U(X) = \emptyset. \quad (8)$$

For this variation to be useful and different than the single radius case, we sample from S , but restrict to points that are close enough to U to reduce it:

$$T(X) = S(X) \cap \{U(X) + R_c\}. \quad (9)$$

The *bias-free* process selects from $T(X)$ uniformly.

This variation is useful to add randomness to initial and continuously parameterized hierarchical samples. Samplings will likely have points that could be removed and still meet the coverage condition (Equation 8). There are more extra points the smaller R_f is compared to R_c . This process provides samplings that are less uniform, i.e., with greater variation in inter-sample distances, than classical MPS. In particular, as the ratio of inhibition and coverage radii grows, the rings in the FFT spectrum of the output are reduced. For a modest ratio, $R_c/R_f = 2$, the radial power oscillations are barely perceptible: the resulting FFT spectrum is much closer to a uniform-random distribution, except for the low frequency component. See Figures 4–10 for examples.

3.1 Edge Length and DT Angle Bounds

We consider a Delaunay triangulation (DT) of our point cloud. The inhibition radius bounds the shortest edge length. The coverage radius bounds the largest empty Delaunay circumcircle. The longest edge length is at most the diameter of that circle. To summarize:

Proposition 1 $|e| \in [R_f, 2R]$ and $R \leq R_c$, where R is the radius of a Delaunay circumcircle.

The Central Angle Theorem provides a relation between the smallest angle α , the shortest edge length $|e|$, and the circumradius R of a triangle. (This has been used to provide quality bounds for separated-yet-dense points since DR's inception [4].)

Proposition 2 $\sin \alpha \geq |e|/2R$.

For example, in a DT of a point set with $R_c = R_f$, we have $\alpha > 30^\circ$. If $R_c = 2R_f$, then $\alpha > 14.4^\circ$.

4 Hierarchical Sampling

4.1 Parameterized radii

Consider a maximal sampling, from either a single disk radius or different inhibition and coverage radii. We scale these radii by t ; e.g., t could be time. For $t \in (0, 1]$ we have $r_f(t) = tR_f$ and $r_c(t) = tR_c$.

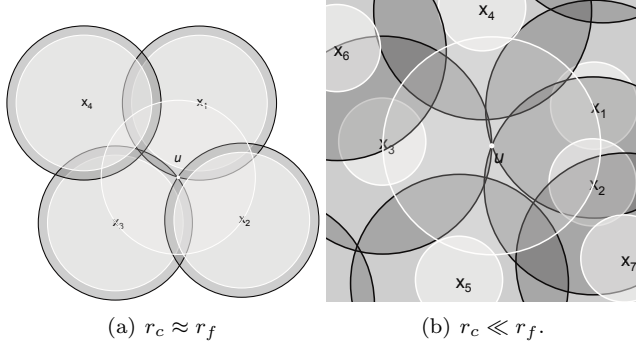


Figure 1: Possible T shapes for two radii when t is reduced to uncover a single point $u = U$. The circumcircle of $\Delta \mathbf{x}_1 \mathbf{x}_2 \mathbf{x}_3$ has center u and radius r_c . T is the part of this circumcircle outside the light r_f disks at x_i .

4.2 Continuous Decrease Refinement

Consider decreasing t continuously from 1 to 0. The sampling becomes non-maximal for some t^* when $U(X) \neq \emptyset$; recall Equation 8. To simplify the discussion assume distinct Delaunay circumradii so the largest one is unique; then at t^* we have that $U(X)$ grows by a single point, a single Voronoi vertex u . A new sample is needed. If $r_f = r_c$ then there is only one place to put the sample, at u , so the process is deterministic. Otherwise, we insert a random point from the set T of free points which will reduce the size of the uncovered set. See Figure 1 for example T shapes. Efficiently selecting a new sample can be done by sampling from a geometric outer approximation to T and resampling if necessary [10, 11].

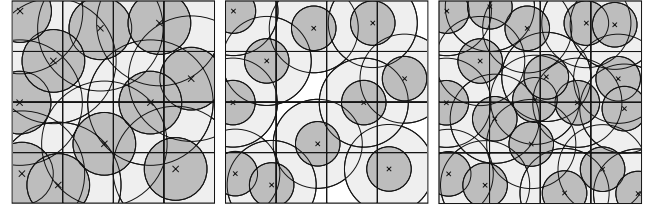
In 2d periodic or infinite domains, we observe that u is the circumcenter of a non-obtuse triangle, which lies inside it. For obtuse triangles, the Delaunay triangle sharing its longest edge has a larger circumsphere, so its center would be uncovered for a smaller t .

DR can be implemented with a priority queue, prioritizing the circumcenters of Delaunay triangles by decreasing radii. A new sample creates new triangles and destroys some old ones, so the queue must be updated. This is essentially the generic Delaunay refinement algorithm with a largest-first queue priority for inserting circumcenters. DR makes no restrictions on the circumcenter insertion order, and the Triangle code [22] takes the opposite approach: processing the smallest triangles first. The main difference is that when an event occurs,

we insert a nearby random point, but DR inserts the point itself (or an off-center, etc.).

4.3 Discrete Decrease Refinement

Consider decreasing t in discrete jumps. For a new value of t , the sampling may be non-maximal, and the same algorithm that generated the initial sampling can be continued to achieve maximality. Figure 2 shows completing a sampling after a jump. Some new samples are inside the light covered region, but, nonetheless, each of their r_c disks reduced the white uncovered area when it was introduced.



(a) $t = 0.8$ end (b) $t = 0.6$ start (c) $t = 0.6$ end

Figure 2: A step in a discrete hierarchy of samplings.

5 Spatially Varying Radii

We aim to produce spatially varying point density according to a sizing function $r(\mathbf{x}) : \Omega \rightarrow (0, \infty)$. A sample satisfies the *empty disk* property, vs. (1), if

$$\forall i < j \leq n, |\mathbf{x}_i - \mathbf{x}_j| \geq f(\mathbf{x}_i, \mathbf{x}_j), \quad (10)$$

and the set of *uncovered points*, vs. (2), is

$$S(X) = \{\mathbf{y} \in \Omega : |\mathbf{y} - \mathbf{x}_i| \geq f(\mathbf{x}_i, \mathbf{y}), i = 1..n\}. \quad (11)$$

Here $f(\mathbf{x}_i, \mathbf{y})$ is a function of $r(\cdot)$ evaluated at a previously accepted sample \mathbf{x}_i and a later candidate sample \mathbf{y} . A candidate is accepted if $|\mathbf{x} - \mathbf{y}| \geq f(\mathbf{x}, \mathbf{y}) \forall \mathbf{x} \in X$ so far. We have four variations:

$f(\mathbf{x}, \mathbf{y}) := r(\mathbf{x})$	Prior-disks,
$f(\mathbf{x}, \mathbf{y}) := r(\mathbf{y})$	Current-disks,
$f(\mathbf{x}, \mathbf{y}) := \max(r(\mathbf{x}), r(\mathbf{y}))$	Bigger-disks,
$f(\mathbf{x}, \mathbf{y}) := \min(r(\mathbf{x}), r(\mathbf{y}))$	Smaller-disks.

(Sphere packings use a sum-of-disks sizing function, $f(\mathbf{x}, \mathbf{y}) = r(\mathbf{x}) + r(\mathbf{y})$.) The f are equivalent for a fixed radius r , but are all distinct for spatially-varying r . Each approach has certain advantages in terms of simplicity, output size, DT quality, and how quickly the sizing function may vary. See Table 1 for a summary, below for proofs for one case, and the extended version of this paper for the other cases.

A variation of Ebeida et al. [10] can efficiently produce a maximal sampling using a flat-quadtrees to capture

Method	Distance Function	Order Independent	Full Coverage	Conflict Free	Edge Min	Edge Max	Sin Angle Min	Max L
Prior	$r(\mathbf{x})$	no	no	no	$1/(1+L)$	$2/(1-2L)$	$(1-2L)/2$	$1/2$
Current	$r(\mathbf{y})$	no	no	no	$1/(1+L)$	$2/(1-L)$	$(1-L)/2$	1
Bigger	$\max(r(\mathbf{x}), r(\mathbf{y}))$	yes	no	yes	1	$2/(1-2L)$	$(1-2L)/2$	$1/2$
Smaller	$\min(r(\mathbf{x}), r(\mathbf{y}))$	yes	yes	no	$1/(1+L)$	$2/(1-L)$	$(1-L)/2$	1

Table 1: Summary of results for spatially varying radii. Points closer than f conflict. Symmetric f provide order independence: any sampling with the order of samples permuted still satisfies the empty disk property. Full coverage means that every point of the domain is inside some sample's r disk. Conflict free means that no sample is inside another sample's r disk. Edge max and min bound the lengths of an edge containing \mathbf{x} in a Delaunay triangulation of X , as a factor of $r(\mathbf{x})$. The Lipschitz constant must be less than max L to bound the maximum DT edge length and minimum DT angle.

the uncovered area. Implementing the conflict condition and coverage checks is simpler for some variations.

There is a limit to how quickly $r(\cdot)$ is allowed to vary. We require that r is L -Lipschitz, i.e., for all $\mathbf{x}, \mathbf{y} \in \Omega$, $|r(\mathbf{x}) - r(\mathbf{y})| \leq L |\mathbf{x} - \mathbf{y}|$ for some constant L . The lengths of DT edges at \mathbf{x} depend not only on $r(\mathbf{x})$ but also on $r(\mathbf{y})$, which can be bounded using L . Some approaches require $L < 1$, others $L < 1/2$. The quality guarantees disappear as L approaches the upper limit. As L approaches zero the quality guarantees smoothly approach those in the uniform case.

Bias-free An alternative to uniform-random is to weight the uncovered set by the local sizing function, i.e., the desired output density. In dimension d ,

$$w(S) = \int_S \frac{1}{r(\mathbf{x})^d} d\mathbf{x}, \text{ and}$$

$$\forall A \subset S(X) : P(\mathbf{x}_{n+1} \in A | X) = \frac{w(A)}{w(S(X))}. \quad (12)$$

While we have not implemented it, one could approximate Equation 12 from values at quadtree corners.

Prior-disk Output Guarantees We justify the edge-length and angle guarantees in Table 1 for **prior-disks**. The proofs for the other criteria are similar and are given in the extended version of this paper.

Proposition 3 *If X satisfies the empty disk property, then for all i, j , $|\mathbf{x}_i - \mathbf{x}_j| \geq \frac{r(\mathbf{x}_i)}{1+L}$.*

Proof. If $i < j$, the empty-disk definition implies $|\mathbf{x}_i - \mathbf{x}_j| \geq r(\mathbf{x}_i)$. Otherwise,

$$r(\mathbf{x}_i) \leq r(\mathbf{x}_j) + L |\mathbf{x}_i - \mathbf{x}_j| \leq |\mathbf{x}_i - \mathbf{x}_j| + L |\mathbf{x}_i - \mathbf{x}_j|$$

by the Lipschitz property and the fact that \mathbf{x}_i satisfies the empty-disk property when it is inserted. \square

Proposition 4 *If X is maximal and T is a resulting Delaunay triangle, then the circumradius $R_T \leq \min\left(\frac{r(\mathbf{y})}{1-L}, \frac{r(\mathbf{x})}{1-2L}\right)$ where \mathbf{y} is the circumcenter and \mathbf{x} is any triangle vertex.*

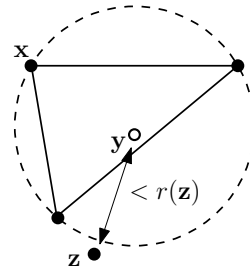


Figure 3: Notation for proofs of circumradii bounds in the Delaunay triangulation of a maximal sampling.

Proof. Since X is maximal, $|\mathbf{z} - \mathbf{y}| \leq r(\mathbf{z})$ for some sample $\mathbf{z} \in X$, where \mathbf{z} is not required to be a vertex of T ; see Figure 3. The Lipschitz property gives

$$|\mathbf{z} - \mathbf{y}| \leq r(\mathbf{z}) \leq r(\mathbf{y}) + L |\mathbf{z} - \mathbf{y}|.$$

Rearranging gives $R_T \leq |\mathbf{z} - \mathbf{y}| \leq \frac{r(\mathbf{y})}{1-L}$. Applying the Lipschitz property again gives,

$$R_T = |\mathbf{x} - \mathbf{y}| \leq |\mathbf{z} - \mathbf{y}| \leq \frac{r(\mathbf{y})}{1-L} \leq \frac{r(\mathbf{x}) + L |\mathbf{x} - \mathbf{y}|}{1-L}.$$

Rearranging again completes the proof. \square

Corollary 5 *If X is maximal, $|\mathbf{x}_i - \mathbf{x}_j| \leq \frac{2r(\mathbf{x}_i)}{1-2L}$.*

Lemma 6 *Suppose X is a maximal sample satisfying the empty disk property. Then all the angles in the Delaunay triangulation are at least $\arcsin\left(\frac{1-2L}{2}\right)$.*

Proof. Let α be an angle in the Delaunay triangulation of X and let \mathbf{x} be the vertex on the edge opposite of α which was inserted *first*. This opposite edge has length at least $r(\mathbf{x})$. Propositions 2 and 4 give $\sin \alpha \geq \frac{r(\mathbf{x})}{2r(\mathbf{x})/(1-2L)} = \frac{1-2L}{2}$. \square

6 Experimental Results

We consider the spectra of distributions generated with the different methods, but similar coverage/inhibition radii. Spectra are analyzed using the Point Set Analysis [21] tool, which generates standardized diagrams, aiding direct comparison. The first panel is the point set. The second panel is the FFT spectrum of the point set with the DC component removed. The third panel

is the radial mean power, which measures the average variation of the second panel's rings' magnitudes.

Figure 4 is for uniform MPS. In the FFT spectrum we see the typical dark central disk surrounded by alternating light and dark rings decreasing in magnitude. Figures 5 and 8 show the PSA results for point clouds generated using different inhibition and coverage radii. The FFT ringing artifacts are dramatically reduced, as is the size of the central disk. Comparing Figures 4 & 5 to 6 & 7 shows that there is little difference in the spectra whether a sampling is generated in a discrete hierarchy over t or directly. Using a large coverage radius yields significantly fewer samples, as seen in Figures 8 and 9.

Figure 11 shows sampling results using the same pseudo-random number sequence over all four spatially varying radii strategies. The experimental results match the theory: the smaller-disk construction yields a larger minimum angle. Figure 12 shows our resampling of a stippled image [14, 24].

7 Conclusions

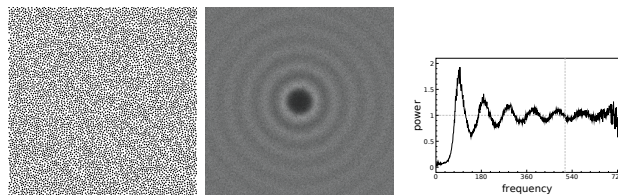
We provide simple definitions for separated-yet-dense random samplings, which are amenable to simple algorithms for generating provable quality point sets and meshes. Intermediate triangulations and Delaunay circumferences are not needed. Of our spatial variations, the smaller-disks approach has the weakest requirements and provides the best quality, but generates the most points. The prior-disks method is the easiest to implement, as it is a minor change to existing MPS algorithms. However, it has the most restrictions on the input and provides the weakest output guarantees.

Acknowledgements

Sandia National Laboratories is a multi-program laboratory managed and operated by Sandia Corporation, a wholly owned subsidiary of Lockheed Martin Corporation, for the U.S. Department of Energy's National Nuclear Security Administration under contract DE-AC04-94AL85000. The research of the authors from University of Texas at Austin was supported in part by NSF grant CNS-0540033 and NIH grant R01-EB004873.

References

- [1] J. Bishop. Simulating the pervasive fracture of materials and structures using randomly close packed Voronoi tessellations. *Comput. Mech.*, 44:455–471, 2009.
- [2] J. E. Bolander and S. Saito. Fracture analyses using spring networks with random geometry. *Eng. Fracture Mech.*, 61(5-6):569–591, 1998.



(a) Point Set (b) FFT Spectrum (c) Radial Power

Figure 4: Uniform MPS with $r = 0.01$ (6656 points).

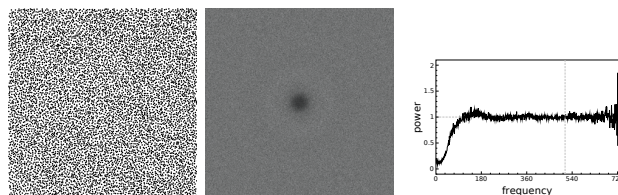


Figure 5: Two-radii, $r_c = 2r_f = 0.01$ (8566 points).

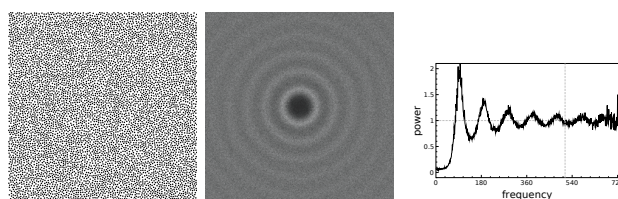


Figure 6: Final sampling in a ten step discrete hierarchy terminating with $r_c = r_f = 0.01$ (6727 points).

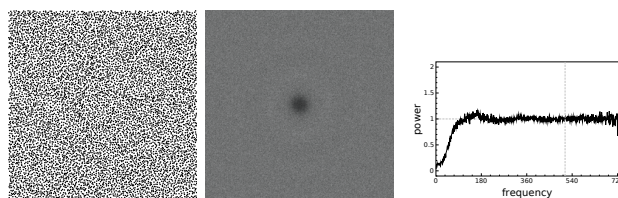


Figure 7: Ten steps to $r_c = 2r_f = 0.01$ (8432 points).

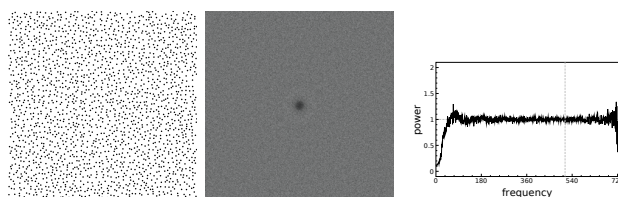


Figure 8: Two-radii, $\frac{r_c}{2} = r_f = 0.01$ (2010 points).

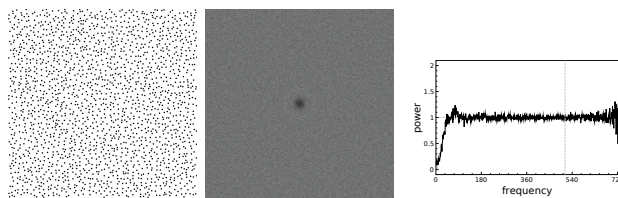


Figure 9: Ten steps to $\frac{r_c}{2} = r_f = 0.01$ (2006 points).

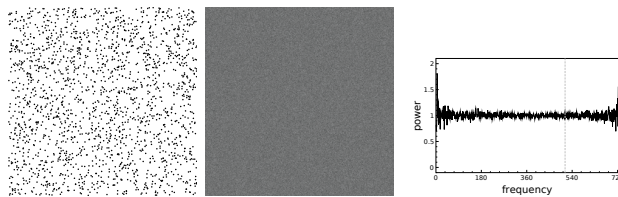


Figure 10: Uniform-random sampling (2010 points).

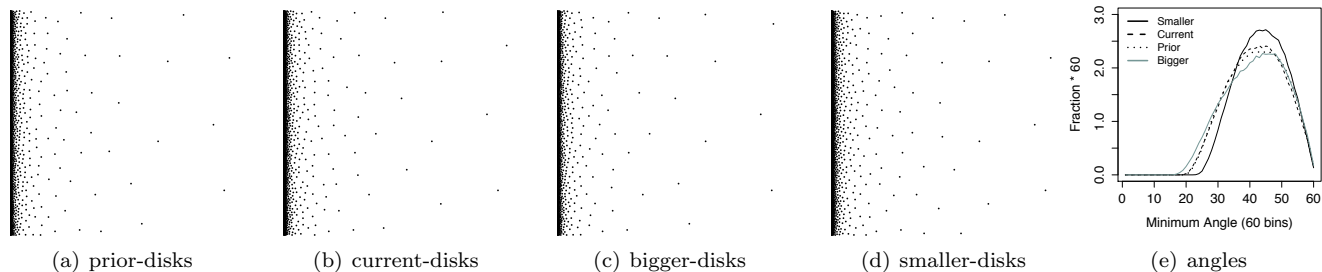


Figure 11: Experimental results for spatially varying radii samplings across conflict criteria. Left, sampling the linear-ramp function, $r(x, y) = 0.001 + 0.3x$. Right, typical DT angle histograms for an r with $L \approx 0.37$.

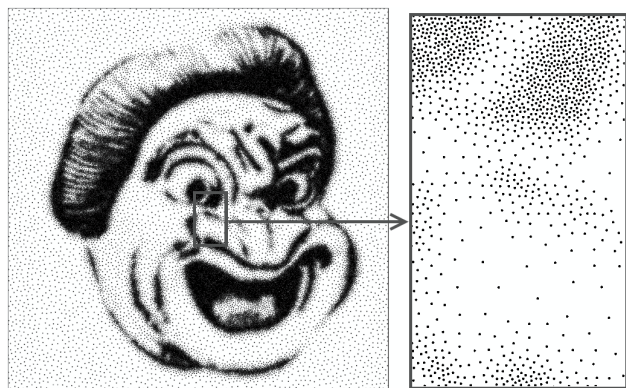


Figure 12: A point cloud was scanned, grayscaled, smoothed for L , then resampled. (Wei, Kopf et al.)

- [3] J. Bowers, R. Wang, L.-Y. Wei, and D. Maletz. Parallel Poisson disk sampling with spectrum analysis on surfaces. *ACM Trans. Graphics*, 29:166:1–166:10, 2010.
- [4] L. P. Chew. Guaranteed-quality triangular meshes. Technical Report 89-983, Department of Computer Science, Cornell University, 1989.
- [5] L. P. Chew. Guaranteed-quality Delaunay meshing in 3D. In *Proc. 13th Symp. Comput. Geom.*, pages 391–393, 1997.
- [6] R. Cook. Stochastic sampling in computer graphics. *ACM Trans. Graphics*, 5(1):51–72, 1986.
- [7] M. S. Ebeida, P. M. Knupp, V. J. Leung, J. E. Bishop, and M. J. Martinez. Mesh generation for modeling and simulation of carbon sequestration process. In *Proc. DOE Scientific Discovery through Advanced Computing (SciDAC) conference*, July 2011.
- [8] M. S. Ebeida and S. A. Mitchell. Uniform random Voronoi meshes. In *Proc. 20th Int. Meshing Roundtable*, pages 258–275, 2011.
- [9] M. S. Ebeida, S. A. Mitchell, A. A. Davidson, A. Patney, P. M. Knupp, and J. D. Owens. Efficient and good Delaunay meshes from random points. *Comput. Aided Des.*, 43(11):1506–1515, 2011.
- [10] M. S. Ebeida, S. A. Mitchell, A. Patney, A. A. Davidson, and J. D. Owens. A simple algorithm for maximal Poisson-disk sampling in high dimensions. *Comput. Graphics Forum*, 31(2):tbd, 2012.
- [11] M. S. Ebeida, A. Patney, S. A. Mitchell, A. Davidson, P. M. Knupp, and J. D. Owens. Efficient maximal Poisson-disk sampling. *ACM Trans. Graphics*, 30(4):49:1–49:12, 2011.
- [12] H. Erten and A. Üngör. Quality triangulations with locally optimal Steiner points. *SIAM J. Sci. Comput.*, 31:2103, 2009.
- [13] P. Foteinos, A. Chernikov, and N. Chrisochoides. Fully generalized 2D constrained Delaunay mesh refinement. *SIAM J. Sci. Comput.*, 32:2659–2686, 2010.
- [14] J. Kopf, D. Cohen-Or, O. Deussen, and D. Lischinski. Recursive Wang tiles for real-time blue noise. *ACM Trans. Graphics*, 25(3):509–518, 2006.
- [15] A. Lagae and P. Dutré. A comparison of methods for generating Poisson disk distributions. *Comput. Graphics Forum*, 27(1):114–129, 2008.
- [16] X.-Y. Li, S.-H. Teng, and A. Üngör. Simultaneous refinement and coarsening: Adaptive meshing with moving boundaries. In *Proc. 7th Int. Meshing Roundtable*, pages 201–210, 1998.
- [17] P. Ljung. Adaptive sampling in single pass, GPU-based raycasting of multiresolution volumes. In *Eurographics*, pages 39–46, 2006.
- [18] M. McCool and E. Fiume. Hierarchical Poisson disk sampling distributions. In *Graphics Interface*, pages 94–105, 1992.
- [19] G. L. Miller, D. Talmor, S.-H. Teng, N. J. Walkington, and H. Wang. Control volume meshes using sphere packing: Generation, refinement and coarsening. In *Proc. 5th Int. Meshing Roundtable*, pages 47–61, 1996.
- [20] J. Ruppert. A Delaunay refinement algorithm for quality 2-dimensional mesh generation. *J. Algorithms*, 18(3):548–585, 1995.
- [21] T. Schlömer. PSA point set analysis. Version 0.2.2, <http://code.google.com/p/psa/>, 2011.
- [22] J. R. Shewchuk. Delaunay refinement algorithms for triangular mesh generation. *Comput. Geom.*, 22(1–3):86–95, 2002.
- [23] D. Vanderhaeghe, P. Barla, J. Thollot, and F. Sillion. Dynamic point distribution for stroke-based rendering. In *Rendering Techniques*, pages 139–146, 2007.
- [24] L.-Y. Wei. Parallel Poisson disk sampling. *ACM Trans. Graphics*, 27(3):20:1–20:9, Aug. 2008.